*lubricants*

MDPI

*Article*

# Partial Surface Texturing in Hydrodynamic Lubrication: A CFD-Based Investigation

**Igal Cohen and Roman Goltsberg ***

Department of Mechanical Engineering, Technion, Haifa 32000, Israel; igalcohen@campus.technion.ac.il
* Correspondence: groman@technion.ac.il

**Abstract:** The present study investigates the effect of partial surface texturing, containing large number of micro-dimples, in lubrication mechanisms. A CFD model is applied to examine the influence of partial surface texturing on pressure and velocity distribution in the flow between mating surfaces with relative motion or pressure drop. Various texturing parameters were analyzed. The results indicate that the equivalent volume step model effectively simulates surface texturing for a wide range of parameters when the untextured surface is in motion or for pressure-drop-induced flows, as surface texturing is less effective than the equivalent volume step by a margin of under 20%. However, when the motion involves the textured surface, surface texturing is found to be significantly less effective than the equivalent volume step and may even lead to detrimental effects, as the gage pressure can be negative. Furthermore, the influence of different parameters of the dimples, such as dimple area density, texturing portion, aspect ratio and dimple depth, on the efficiency reduction of surface texturing compared with the step model is discussed.

**Keywords:** partial surface texturing; CFD modeling; micro-dimples; motion-induced flow

## 1. Introduction

Tribology is the science dealing with the friction, lubrication and wear of interacting surfaces. Contacting or near contacting surfaces in relative motion in the presence of a lubricant can be found in a variety of machine elements: hydrodynamic bearings, mechanical seals, piston–cylinder systems, gearing, etc. Generating separating force between the surfaces is the principal problem of lubrication. The separating force can be generated by external pressure (generally by a pump) also termed as hydrostatic lubrication or by an internal, self-acting mechanism, also termed as hydrodynamic lubrication. In hydrodynamic lubrication, the separating force is generated by the time or spatial variation of the lubricant fluid film geometry. One approach involves the convergence of the fluid film in the direction of the flow, generating a pressure rise in relation to the operating pressure to ensure the conservation of the mass flow rate.

The variation in space can also be implemented through surface texturing. It is well known that the suitable texturing of the mating surfaces, moving relative to each other, can improve the tribological performance, for example reducing friction and wear, damping noise and vibration and in some applications preventing physical contact and thereby reducing the energy loss in mechanical systems [1–3]. The use of texturing techniques allows obtainment of pressure generation through microstructure instead of a macro-geometry [4], which may not be practical at a scale of microns.

Various texturing techniques can be used, including machining, ion beam texturing, etching techniques and laser texturing. It seems that laser surface texturing (LST) offers the most promising concept of all the practical micro-surface texturing methods [5] due to its high flexibility and accuracy. The implementation of LST is fast, cheap and clean to the environment [6].

check for updates

**Citation:** Cohen, I.; Goltsberg, R. Partial Surface Texturing in Hydrodynamic Lubrication: A CFD-Based Investigation. *Lubricants* **2023**, *11*, 395. https://doi.org/10.3390/lubricants11090395

Received: 14 August 2023
Revised: 4 September 2023
Accepted: 8 September 2023
Published: 12 September 2023

LST in the form of the spherical segment dimples is an effective method for the improvement of tribological performance [7]. In addition to generating a separating force in the case of full lubrication, each dimple can serve as a micro-reservoir or a micro-trap for wear debris in case of starved lubrication [8]. However, despite the promising results, universal guidelines for optimum texturing cannot be found in the literature [3]. The optimum parameters for the texturing that can be found in the literature focus on specific applications and operating conditions. Since improper design of the texturing may lead to undesired pressure reduction or provide an unsatisfying improvement [3], there is a great interest in gaining a general understanding about the influence of textured surfaces on lubrication applications.

The texturing can be applied on an entire surface, termed "full texturing", or on a portion of the surface, termed "partial texturing". Full texturing can enhance the tribological performance due to the cavitation phenomena, as was shown experimentally and analytically in [9] for a laser-textured mechanical seal face. It can also reduce the wear rate under mixed and dry lubrication as was shown experimentally in [10].

On the other hand, since partial texturing is applied only on a portion of the surface, the average clearance between the surfaces in the textured zone is higher the clearance in the untextured zone and therefore it effectively creates a converging clearance. In [4], it was suggested to use the removal of material, through texturing, as a method to produce an effective step or slope profile.

In [11], Etsion and Halperin theoretically and experimentally demonstrated the effectiveness of partial texturing in enhancing the tribological performance of a hydrostatic mechanical seal. In [12], Brizmer et al. investigated the effect of partial surface texturing for a thrust bearing. It was shown that partial surface texturing leads to a bi-linear pressure distribution that is similar to a Rayleigh step bearing. They examined the influence of the texturing parameters such as dimple depth, texturing portion and dimple area density (the ratio between the total area covered by dimples and the area of the textured zone) on the load-carrying capacity. It was found that, for optimal results, the dimple area density should be as high as possible and that the dimple depth and the textured portion have an optimum depending on the operation conditions. In [13], Kligerman et al. reached similar conclusions for piston rings. Additionally, optimum dimple parameters, in a partial texturing arrangement, were found for various operation conditions.

Despite the similarity that has been reported in the literature between partial texturing and Rayleigh step bearing, a quantitative comparison cannot be found. Since the pressure distribution for Rayleigh step bearing has an analytical solution based on the Reynolds equation (see Ref. [14]), it is of great interest to perform a quantitative comparison, as this would provide, if proven correct, an efficient means to predict the pressure distribution for partial surface texturing.

The pressure distribution for partial surface texturing, unlike Rayleigh step bearing, cannot be solved analytically. Additionally, employing the Reynolds equation to obtain the pressure distribution in surface texturing, which is characterized by substantial changes in the clearance, may yield incorrect results due to the violation of the negligible curvature assumption of the Reynolds equation.

The applicability of the Reynolds equation for surface texturing in lubrication problems was studied in the past [3,15–17]. In [3], Gropper remarked that a textured surface is characterized by surface discontinuities, which is a major numerical challenge that cannot be handled by the Reynolds equation. In [15], Dobrica and Fillon found that for textured sliders of infinite width with aspect ratios (dimple length/dimple depth) less than 10 (deep dimples), the Reynolds equation is not valid, even for low Reynolds numbers. In [16], it was concluded that for a dimple depth having the same order of magnitude as the clearance, the difference between the CFD (computational fluid dynamics) model and the Reynolds equation results for the load carrying capacity can be up to 20%. In [17], the validity of the Reynolds equation for modeling the flow in a single three-dimensional spherical dimple given to a pressure drop was studied. It was found that the Reynolds equation

cannot be used for big clearances (more than 5% of the dimple radius) or for relatively high pressure drops. Hence, a more suitable tool for more reliable results must be used to analyze partial texturing. More reliable results can be obtained by using CFD. The CFD method is based on the Navier–Stokes equations and therefore, it does not consider most of the assumptions of the Reynolds equation. There are cases that have been reported in the literature of lubrication applications in which the results obtained by the Reynolds equation are not reliable due to a violation of the Reynolds equation's assumptions. For instance, in [18–20], it was shown that the CFD method can predict the phenomena that were observed experimentally and cannot be predicted by the Reynolds equation. On the other hand, generally, the use of a CFD model is complex and expensive (by means of computation resources) compared with Reynolds equations. In order to overcome the constraints of the Reynolds equation, CFD models have been applied in several studies on surface texturing. In [21,22], CFD models of a single dimple were used in order to examine the tribological performance of a single-dimple-textured surface in hydrodynamic lubrication. The optimum parameters including dimple depth, film thickness and dimple area density were found for different operation conditions.

However, as Dobrica and Fillon remarked [15], a CFD model of a single dimple does not consider the interaction between neighboring dimples and hence is not suitable for modeling textured surfaces. This is particularly true for partial texturing cases. Indeed, in [23], a CFD model of a single elliptical dimple with periodic boundary conditions and a more complex model of several scattered dimples were compared, and significant differences were found. The authors showed that the model with a single dimple cannot be used to predict the results for several dimples. In [24], a more advanced CFD model of several dimples with periodic and symmetric boundary conditions was used to investigate the tribological performance of a fully textured surface. It was shown both experimentally and theoretically that appropriate texturing can obtain considerable friction reduction.

However, even though several dimples were used in some of the above-mentioned models, they can only be used to simulate full texturing and hence the obtained insights are not applicable for partial surface texturing cases. In order to simulate partial texturing, a more realistic model with multiple dimples should be used. However, to the best of the authors' knowledge, there are no CFD-based studies with multiple dimples and all the existing literature results for partial texturing have been obtained by using the Reynolds equation.

Moreover, in the majority of both theoretical and experimental studies on surface texturing, the textured surface is static and the untextured surface is moving. The sole study that examined the case of a moving textured surface, to the best of authors' knowledge, is [21]. The authors of [21] examined the lubrication behavior of journal bearing with dimples by using a CFD model of a single dimple. It was found that the movement of the textured surface led to a smaller friction force and friction coefficient than the movement of the untextured surface.

In the present study, a CFD model is used to obtain the pressure distribution and velocity field between two mating surfaces with relative motion, where one of the surfaces is partially textured and has a realistic number of spherical dimples (dozens to hundreds in the longitude direction). The goal of the present study is to examine the probability of using an equivalent volume step model in order to estimate the influence of the texturing on the pressure distribution, as was suggested in [12]. A design tool is provided to convert the texturing parameters to an equivalent volume step. In addition, the fluid flow and the pressure distribution in the textured zone are examined in order to understand the influence of various texturing parameters, such as the dimple aspect ratio, area density and texture portion, on the flow and the applicability of the simplified step model. An improved design tool, based on the volume of the texturing and on the influence of the parameters, is provided in order to predict the pressure distribution of the flow for the partial texturing. Obtaining the pressure distribution is important as it allows the calculations of the load

carrying capacity and the flow rate between the mating surfaces. These fundamental parameters are critical for a wide range of lubrication applications.

## 2. Theoretical Background

In the following, the models for the partial surface texturing and the Rayleigh step bearing are presented. In addition, the analytical solution for the pressure distribution and the mass flow rate for Rayleigh step bearing are described.

### *2.1. Rayleigh Step Bearing*

Figure 1 illustrates a mid-cross-section of two mating surfaces (there is no contact between the surfaces), where one of them is partially textured, in relative motion with fluid flow between them, given to a pressure drop (from the inlet to the outlet). The pressures at the inlet and the outlet are denoted by $P_1$ and $P_1$, respectively, and the longitude velocity is denoted by $U$. The velocity can be applied either on the textured surface or on the untextured surface (the flow direction of the fluid is the same for both cases). The texturing is located close to the inlet and by that it effectively creates a converging clearance. The length of the surfaces is $L$. The nominal gap is denoted by $C$ and the texturing portion is $\alpha$. The longitude coordinate is denoted by x and the coordinate in the gap direction is denoted by y.

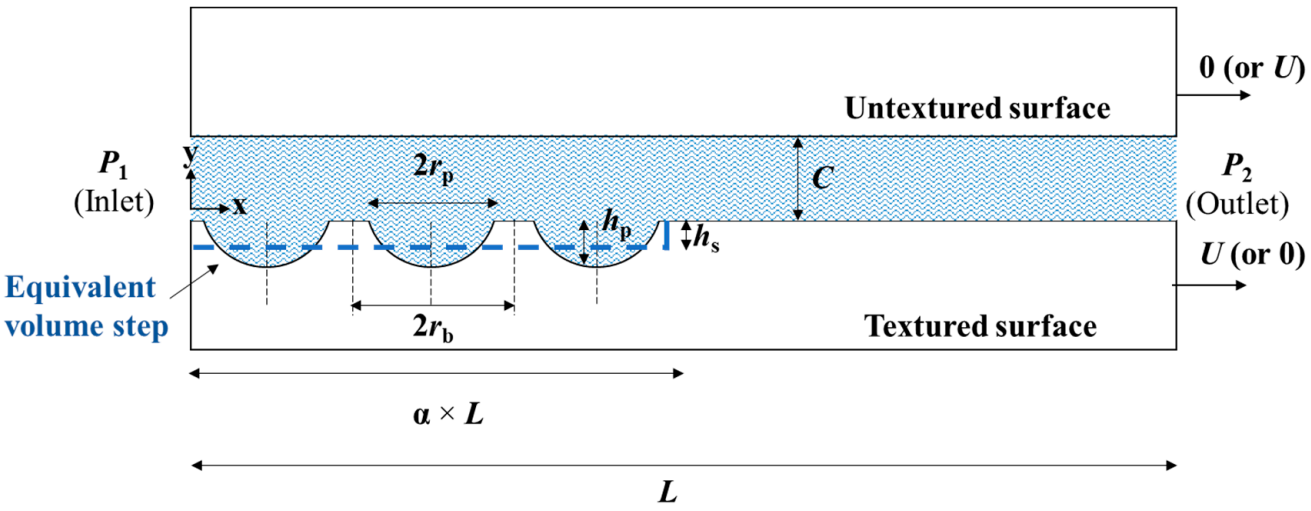


**Figure 1.** A mid-cross-section of the surfaces.

In order to compare between the solution of the partial texturing and the step profile, the volume of the dimples is converted to an equivalent volume of the step, whereas the texturing portion, $\alpha$, does not change. The step is characterized by two parameters—the step length, $\alpha \times L$, and the step depth, $h_S$, as depicted in Figure 1 by the blue dashed line.

The pressure $p(x)$ distribution for the equivalent step can be obtained by solving the one-dimensional, steady-state form of the Reynolds equation for an incompressible fluid in laminar flow, which is given by [14]:

$$\frac{\partial}{\partial x}(h^3\frac{\partial p}{\partial x}) = 6\mu U\frac{\partial h}{\partial x} \tag{1}$$

where $h(x)$ is the local value of the film thickness (gap) and $\mu$ is the viscosity of the fluid. The boundary conditions for the pressure field are given by:

$$\begin{aligned} p(x=0) &= P_1 \\ p(x=L) &= P_2 \end{aligned} \tag{2}$$

An analytical solution for the pressure distribution, based on mass flow conservation, can be found in [14]. The solution for the pressure distribution is bi-linear and can therefore be characterized by the pressure at the end of the texturing portion, which represents the location where the fluid film discontinuity occurs within the step. It is denoted by $P_{c,S}$ and is given by [14]:

$$P_{c,S} = \frac{12\mu\alpha(1-\alpha)L}{(1-\alpha)(C+h_S)^3+\alpha C^3}\frac{h_S}{2}U + \frac{p_1(1-\alpha)(C+h_S)^3+p_2\alpha C^3}{(1-\alpha)(C+h_S)^3+\alpha C^3} \quad (3)$$

The mass flow rate per unit of width of the surface is denoted by $q$ and is given by [14]:

$$q = \rho\left(\frac{1}{2\mu}\frac{p_{c,S}-p_2}{(1-\alpha)L}\frac{C^3}{6} + \frac{C}{2}U\right) \quad (4)$$

where $\rho$ is the density of the fluid.

### *2.2. Partial Surface Texturing (Dimples)*

The dimples are characterized by four parameters: length of treatment—$\alpha \times L$; dimple base radius—$r_p$; imaginary square cell length—$2r_b$; and dimple depth—$h_p$; these are presented in Figure 1. The model depicted in Figure 1 is at the width of an imaginary square cell length. Each dimple is modelled by a spherical segment that is located in the center of an imaginary square cell. The imaginary square cell length and the dimple base radii determine the dimple area density, $S_p = \pi r_p^2/4r_b^2$, which was shown to have a significant effect on the tribological performance [25].

Another important parameter that was shown to have a significant effect on the flow for partial texturing is the Reynolds number [22]. In hydrodynamic lubrication, it is more convenient to discuss the reduced (sometimes also denoted in the literature as modified) Reynolds number [26], $Re^*$, which is a dimensionless number that describes the ratio between inertia and viscous forces and also considers the ratio between the dimensions of the solved geometry when one dimension is significantly smaller than the others. It is given by [26]:

$$Re^* = \frac{\rho U C^2}{L\mu} \quad (5)$$

The influence of $Re^*$ on the flow is examined in the following sections.

## 3. Numerical Model

The finite-volume model from the commercial ANSYS FLUENT 2023 software was used to solve the problem. The 3D geometry and the mesh design of the fluid flow for the current model, as depicted in Figure 1, are presented in Figure 2. The upper surface corresponds to the fluid layer adjacent to the untextured surface. The bottom surface is the fluid layer adjacent to the textured surface. The surfaces at the ends of the x-direction are the inlet and the outlet. The side surfaces are part of the fluid flow and are assumed to be symmetric, simulating multiple columns.

The current model allows us to solve various hydrodynamic lubrication applications with textured surfaces. A similar model, based on the Reynolds equation, was used in [12] for pad thrust bearing, in which the symmetry was used to simulate an infinitely long slider (in the radial direction). In [7,13], the symmetry was used in the circumferential direction, simulating piston rings, and in [25], it was simulating a circumferential gas seal. It can also be used to simulate a ringless piston in a piston cylinder system (see [20,27]). In [9,11], the symmetry was used in the circular direction, simulating a mechanical seal.

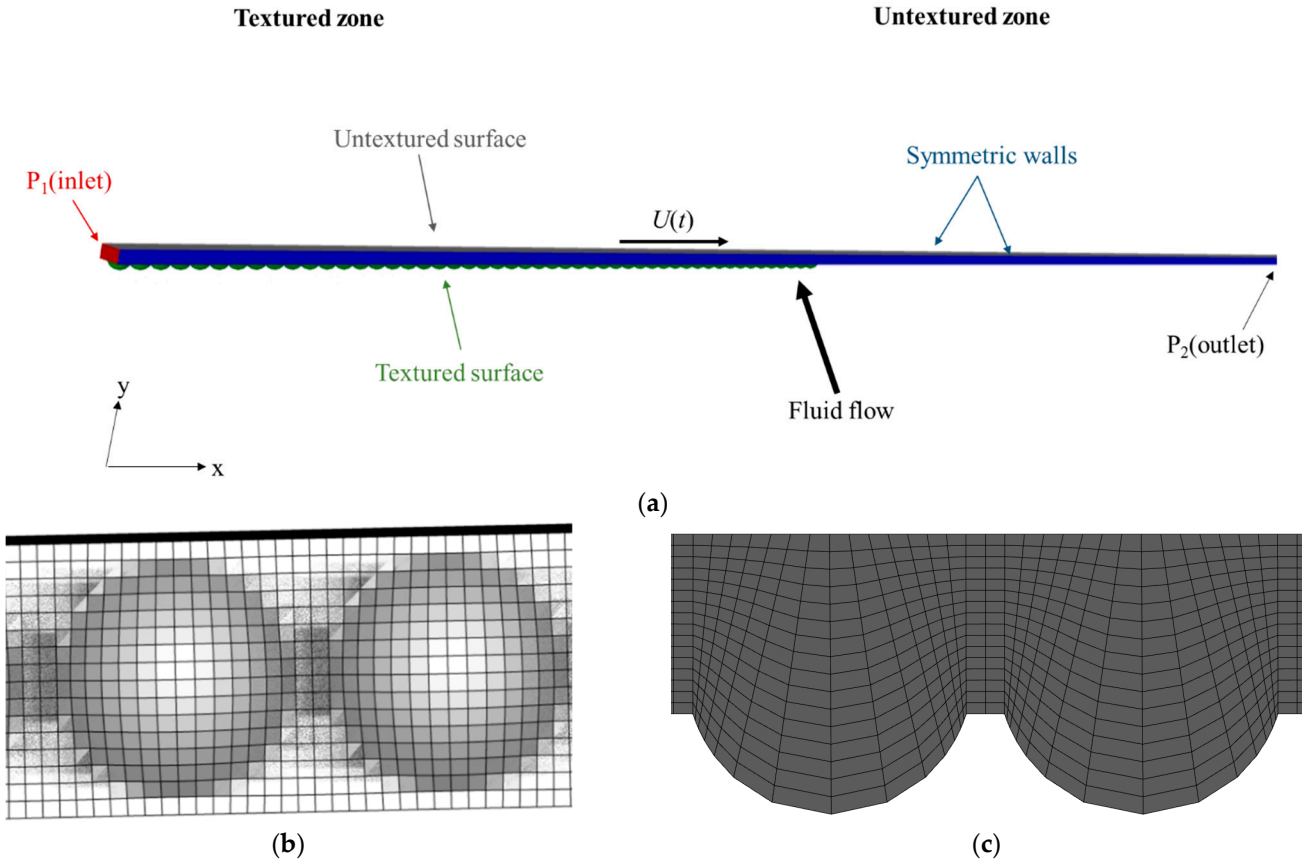


**Figure 2.** The geometry and the mesh design of a typical model for (**a**) an isometric view of the 3D model of the entire domain, (**b**) the bottom-view and (**c**) the side-view of mid-cross-section for two dimples.

The mesh for each imaginary square cell has 16 × 16 elements and 16 layers in the thickness (gap), as presented in Figure 2b,c. The untextured zone has about 100 elements in the axial direction, 16 elements in the width direction and 16 layers in the thickness. Increasing the number of elements by a factor of two changes the results for the pressure distribution by less than 1%.

The main assumptions of the model are:

1. The fluid flow is laminar and fully developed.
2. The fluid is incompressible and Newtonian with constant viscosity (isothermal).
3. The surfaces are rigid bodies.
4. No slip and no penetration conditions are applied to the surfaces.
5. The surfaces are smooth (except for the texturing), in other words, the roughness is not considered.
6. No cavitation takes place due to a high operating pressure.

The fifth assumption enables obtaining results that can be compared with the findings in the literature. The last assumption is essential since the main goal of the current study is to compare between partial texturing and an equivalent volume step in which cavitation does not occur. The assumption is reasonable because in partial texturing the pressure is lower than the inlet pressure only at the first dimple (see [3]); therefore, for the majority of applications, cavitation will not occur. For the full texturing, the surface texturing is beneficial due to the cavitation phenomena; therefore, the last assumption must be dropped.

A three-dimensional, steady, pressure-based solver for a laminar flow was employed. The "SIMPLE scheme" was used for the pressure–velocity coupling, whereas the pressure was interpolated by the second-order scheme. Pressure inlet and pressure outlet boundary conditions were used for the inlet ($P_1$) and outlet ($P_2$) surfaces depicted in Figure 2.

The boundary conditions for the velocity field are given by:

$$\begin{matrix} u(y=0)=U \\ u(y=C)=0 \end{matrix} \text{ or } \begin{matrix} u(y=0)=0 \\ u(y=C)=U \end{matrix} \tag{6}$$

where $y = 0$ is the textured surface location and $y = C$ is the untextured surface location. To apply the boundary conditions, stationary wall and moving wall (x-direction only) boundary conditions were used for the textured and untextured surfaces, respectively, or vice versa. Symmetry boundary conditions were used for the side surfaces.

To validate the model, a comparison with the literature for the full-texturing model was made and is presented in the following section. In this case, the volume of fluid (VOF) method and the Schnerr–Sauer cavitation model were used to evaluate the phase interactions. For more information on the governing equations that were solved by the numerical model, the reader is referred to [28].

## 4. Results

In the following section, the numerical model of the current study is validated with experimental and numerical results from the literature. In addition, since the Reynolds equation is linear, by assuming there is no cavitation the influence of $U$ and $\Delta P = P_1 - P_2$ on the local pressures is linear and commutative. In other words, the resulting force (integral of the local pressures) for the case with pressure drop and velocity is equal to the combination of the resulting forces for the two separate cases. Therefore, the discussion is separated into the velocity-induced flow and the pressure-drop-induced flow.

Moreover, doubling the velocity will double the resulting force and applying velocity in the opposite direction will result in the same force in the opposite direction. The current numerical model shows similar results for small values of the reduced Reynolds number, $\mathrm{Re}^* < 0.01$, which includes the majority of lubrication applications [26].

As mentioned, the results of the partial texturing are compared with the results for an equivalent volume step having the same length of treatment. Therefore, to calculate the step depth, $h_S$, the volume of the step should be equal to the volume of the dimples.

The volume of each dimple, $V_p$, is given by:

$$V_p = \frac{\pi}{6} h_p (3r_p^2 + h_p^2) \tag{7}$$

The volume of each imaginary square, $4r_b^2 h_S$, should be equal to the volume of the dimple and therefore:

$$h_S = \frac{V_p}{4r_b^2} \tag{8}$$

### *4.1. Validation of the Numerical Model*

To validate the numerical model presented here, a comparison with some experimental results from [9] and theoretical results from [9,12] are shown below. In [9], a laser-textured mechanical seal face was used for demonstrating the potential of surface texturing. An application of sealing water was selected. The stationary textured ring was axially loaded and the upper untextured ring was rotating at 4000 rpm (average velocity of 7 [m/s] in the circumferential direction). The clearance and the temperature of the water (which affects the viscosity) were measured and substituted into the Reynolds equation to obtain the theoretical results of the average pressure. Table 1 summarizes the input data that were used for this comparison. More information on the experiment (e.g., test setup, materials, motion, conditions, etc.) and the theoretical Reynolds-equation-based model can be found in [9]. The theoretical results were compared with the experimental results. Figure 3 presents the average pressure as a function of the clearance. The results obtained from the Reynolds equation (in reference [9]) are indicated by the solid line, those from the CFD model (current study) are indicated by the dashed line and those from the experimental

results are indicated by the circle markers. Since the measured temperature of the water is not given, it was assumed to be 40°. The CFD model used in the current study shows good agreement with the experimental results. The differences are less than 5% (the experimental deviation was not mentioned in [9]. The accuracy of the results obtained by the CFD model is significantly better than the result obtained using the Reynolds equation.

**Table 1.** Input parameters for the comparison.

| Parameter | Ref. [9] | Ref. [12]—Partial Texturing | Ref. [12]—Full Texturing |
|---|---|---|---|
| Length, $L$ (mm) | 5.75 | 5 | 5 |
| Clearance, $C$ (μm) | 1–5 | 20 | 20 |
| $P_1$ (MPa) | 0 | 0 | 0 |
| $P_2$ (Mpa) | 0 | 0 | 0 |
| Velocity, $U$ (m/s) | 7 | 1 | 1 |
| Viscosity, μ (Pa×s) | 0.0007 | 0.0022 | 0.0022 |
| Density, ρ (Kg/m$^3$) | 998 | 925 | 925 |
| Imaginary square length, $2r_b$ (mm) | 0.188 | 0.5 | 1.0 |
| Dimple base diameter, $2r_p$ (mm) | 0.095 | 0.4 | 0.4 |
| Dimple depth, $h_p$ (μm) | 6 | 26 | 26 |
| Texturing portion, $\alpha$ | 1.0 (full texturing) | 0.6 | 1.0 (full texturing) |
| Dimple area density, $S_p$ | 20% | 50% | 13% |
| Number of dimples | 31 | 6 | 5 |

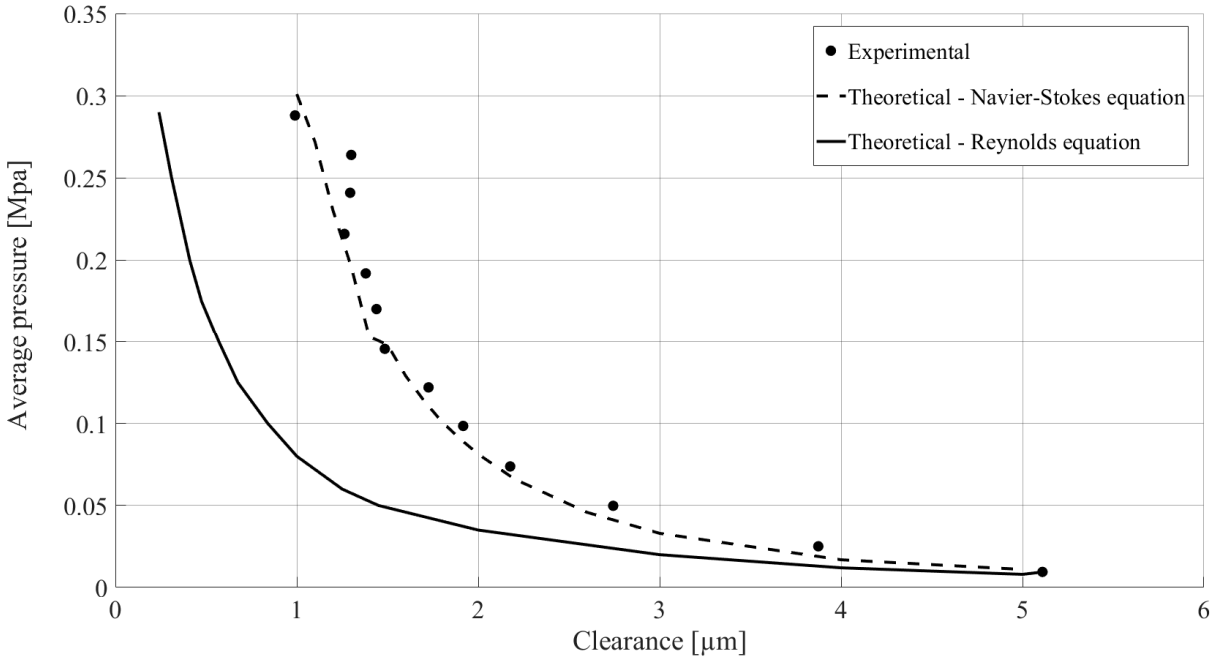


**Figure 3.** Comparison between experimental and theoretical results of average pressure vs. clearance, $C$. Experimental and Reynolds equations results from [9].

In [12], the Reynolds equation with the same analytical model as in [9] was used to find the pressure distribution and the load carrying capacity for a laser surface partially

textured parallel thrust bearing. In Figure 4, a typical distribution of local pressure for partial and full texturing along the center line is presented. The dimensionless coordinate is given by $x^* = r_p/L$, and the dimensionless pressure is given by $p^* = 2r_p p/3\mu U$. The results obtained from the Reynolds equation (in [12]) are indicated by the solid line and the results obtained from the Navier–Stokes equation (current study) are indicated by the circle markers. The pressure distribution for the partial texturing is similar (less than a 4% difference). However, for the full texturing, similar to the previous case discussed in Figure 3, the difference between the models is more significant. From both cases it seems that the current numerical model is valid. In addition, it seems that neglecting the roughness effects (the fifth assumption) is justified.

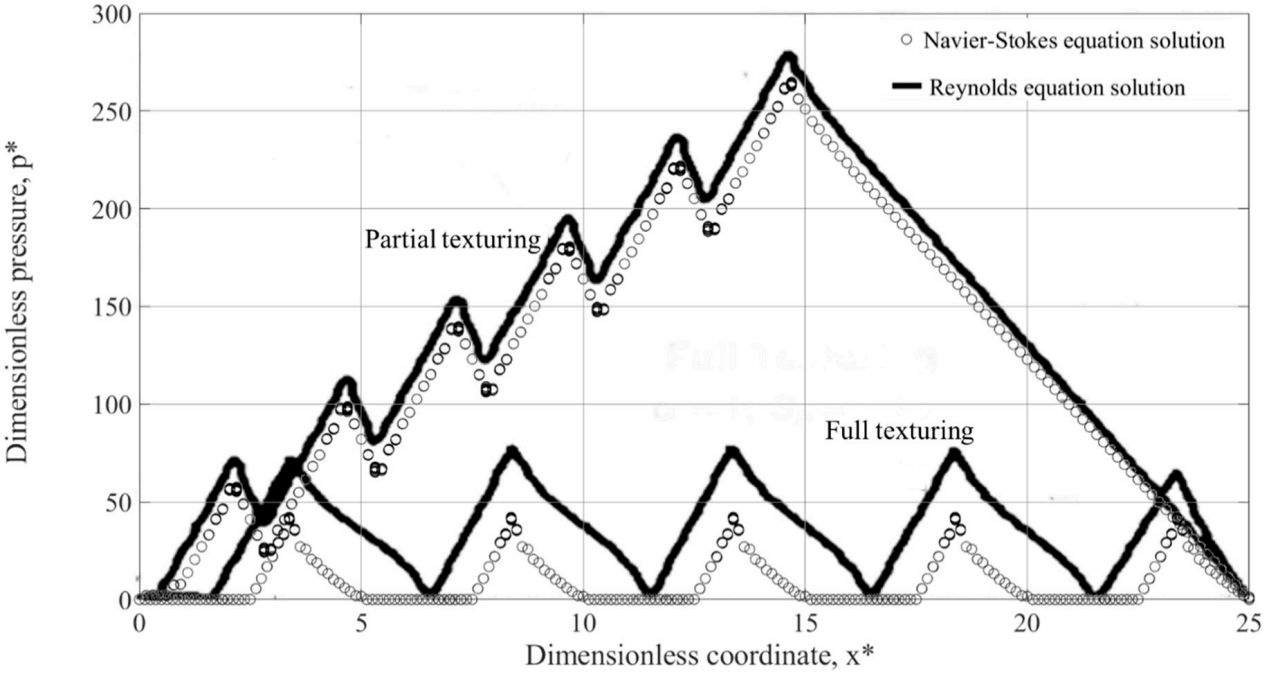


**Figure 4.** Comparison between the Reynolds equation and CFD model of typical distributions of local pressure for partial and full texturing.

### *4.2. Velocity Induced Flow*

In this section, $\Delta P = 0$ and $U = 1[\mathrm{m/s}]$ from left to right (see also Figure 2). Figure 5 presents typical pressure distributions within the fluid for the case of a moving textured surface (the untextured surface is stationary) using the blue circle markers, a moving untextured surface (the textured surface is stationary) using the orange markers and for the equivalent volume step using a solid line (the CFD results for the step show good agreement with the analytical solution obtained by Equation (3)). Two sets of typical parameters are presented. The dimples for the first set are shallow and for the second set are deep. The parameters that were used are summarized in Table 2. The pressure for all the nodes in the x-direction is presented. The pressure gradient inside each dimple is similar to the other dimples. Therefore, even though there is a 3D complex pressure distribution within each dimple, the overall pressure distribution in the textured zone is linear and the overall pressure distribution is bilinear, which is similar to the pressure distribution for Rayleigh step bearing. Therefore, it can be characterized by the pressure at the end of the textured zone and is denoted by $P_{c,D}$. In addition, $P_{c,D}$ can be used to calculate the mass flow rate by substituting it into Equation (4). The numerical results for the mass flow rate, obtained by ANSYS Fluent, showed good agreement with substituting $P_{c,D}$ into Equation (4) (less than 1% difference).

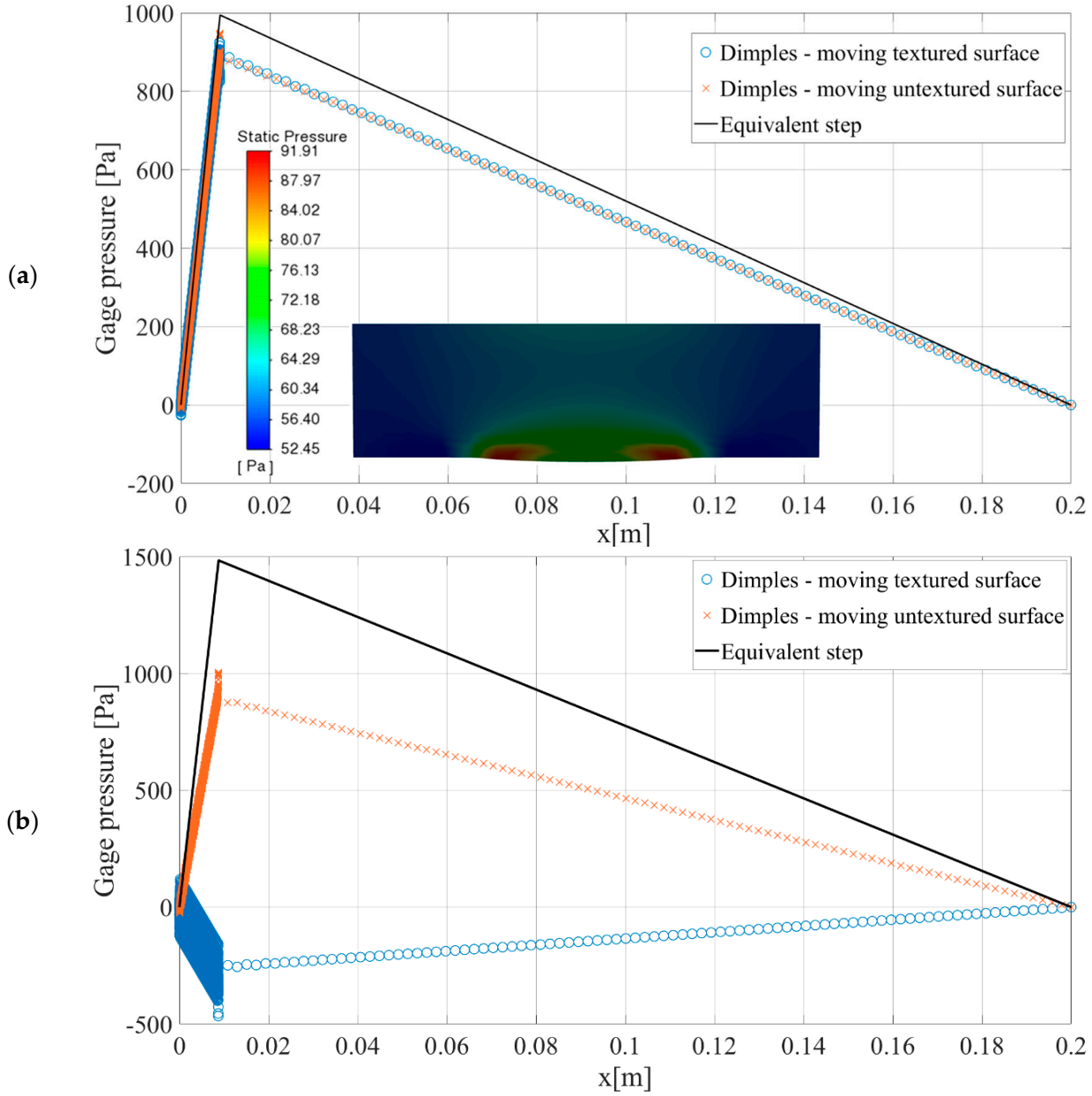


**Figure 5.** Typical distributions of local pressure for (**a**) $C = 50[\mu m]$, $h_p = 4[\mu m]$ and typical perpendicular plane at one of the dimples (**b**) $C = 80[\mu m]$, $h_p = 30[\mu m]$. Dimple texturing and equivalent step.

In addition, the contours of the pressure distribution of a typical plane of the texturing zone that is perpendicular to the x-direction for the moving textured surface case is presented (for the shallow dimples). The results show that there is a pressure difference in the gap direction in the textured zone, unlike the Reynolds equation's assumption in which there is no pressure variation in the gap direction. These results are compatible with the results in [19], in which there was a pressure variation in the gap direction for lubrication applications.

For the first set of parameters with the high aspect ratio (shallow dimples), the correlation between the surface texturing for both moving surfaces and the equivalent step is good. Even though the surface texturing is less effective, the difference is small and the equivalent step can be used for simulating surface texturing.

**Table 2.** Input parameters for the problem.

| Parameter | First Set (Figure 5a) Shallow Dimples | Second Set (Figure 5b) Deep Dimples |
|---|---|---|
| Length, $L$ (m) | 0.2 | 0.2 |
| Viscosity, $\mu$ (Pa$\times$s) | 0.0022 | 0.0022 |
| Density, $\rho$ (Kg/m$^3$) | 900 | 900 |
| Imaginary square length, $2r_b$ (mm) | 0.174 | 0.174 |
| Dimple base diameter, $2r_p$ (mm) | 0.153 | 0.153 |
| Texturing portion, $\alpha$ | 0.045 | 0.045 |
| Dimple area density, $S_p$ | 60% | 60% |
| Number of dimples | 50 | 50 |
| Clearance, $C$ ($\mu$m) | 50 | 80 |
| Dimple depth, $h_p$ ($\mu$m) | 4 | 30 |
| Aspect ratio, $2r_p/h_p$ | 38 | 5 |

For the second set of parameters with the low aspect ratio (deep dimples), the surface texturing is significantly less effective than the equivalent step, particularly for the moving textured surface; therefore, the equivalent step cannot be used for simulating surface texturing. The moving textured surface results in negative gage pressure and, hence, despite the effective converging fluid film created by the texturing, the texturing in this scenario has a negative impact on the tribological performance.

Figure 6 presents the typical velocity vectors inside a dimple for both sets of parameters in the case of a moving textured surface (the velocity vectors for all the dimples are similar). For the first set, the dimples are shallow and the velocity vectors are nearly parallel to the x-direction. Therefore, for this case, even for a moving textured surface, there is a good agreement with the results for the equivalent step. The agreement between the results for the moving textured and untextured surfaces is consistent with the assumptions of the Reynolds equation, in which the pressure distribution is determined by the flow direction of the fluid and is not dependent on which surface is moving. For the second set, in which the dimples are deep, the velocity vectors show high velocities in the gap direction (it can reach up to 50% of the x-velocity). The high velocities in the gap direction prove that the Reynolds equation in which the velocity in the gap direction is neglected is not valid for this case. The inapplicability of the Reynolds equation for this case may explain the difference between the texturing and the equivalent step.

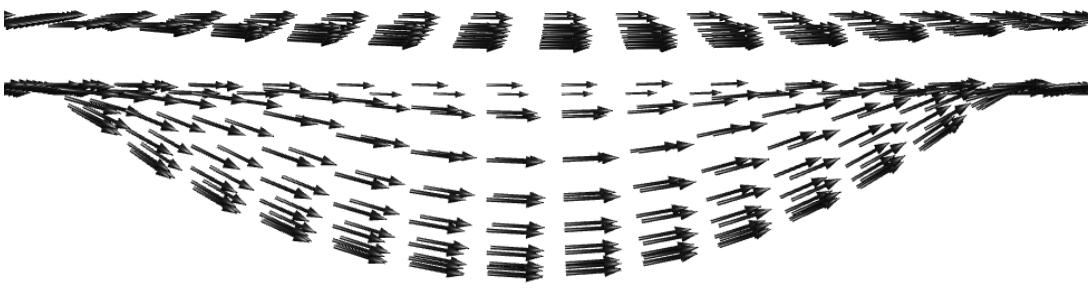


**Figure 6.** The velocity vectors (indicated by arrows) at the dimple for (**a**) $C = 50[\mu m]$, $h_p = 4[\mu m]$ and (**b**) $C = 80[\mu m]$, $h_p = 30[\mu m]$.

Figure 7 further emphasizes and explains the difference between the shallow and deep dimples. It presents contours of the x-velocity in half-planes perpendicular to the x-direction for both sets of parameters. The half-planes are located between two consecutive dimples and in the middle of the dimples. For the first set, the contours are equally spaced, e.g., close to the linear distribution of the x-velocity, which similar to the expected results from the Reynolds equation. For the second case, the contours of the x-velocity close to the textured surface (the bottom edge) are very dense. That indicates a high velocity gradient close to the textured surface. The high velocity reduction causes a reduction of the mass flow rate (integral of the x-velocity on the plane). Since the mass flow rate at the textured and untextured zones is conserved, a negative pressure drop in the x-direction that increases the mass flow rate in the textured zone is created. Therefore, for this case, the texturing is detrimental.

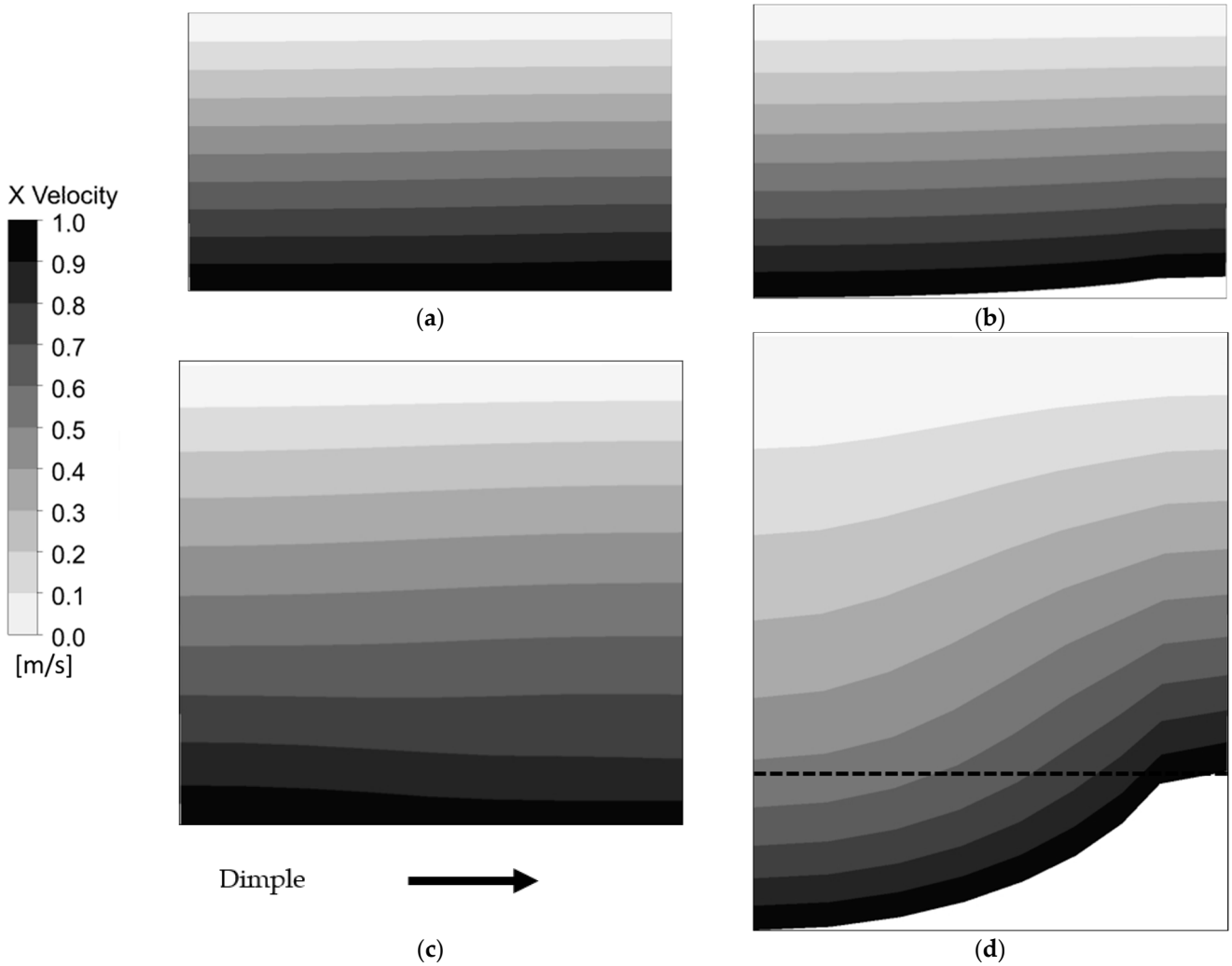


**Figure 7.** Contours of the x-velocity for (**a**) $C = 50[\mu m]$, $h_p = 4[\mu m]$ between the dimples and (**b**) middle of the dimple. (**c**) $C = 80[\mu m]$, $h_p = 30[\mu m]$ between the dimples and (**d**) middle of the dimple.

The use of the CFD model rather than the Reynolds equation enables investigation of the influence of the Reduced Reynolds number $Re^* = \rho U C^2 / L\mu$ on the results. In the following, the influence of $Re^*$ on the pressure distribution for the two sets of parameters mentioned above is examined. Figure 8a presents the effect of $Re^*$ on $P_{c,D}$ for the two sets of parameters in both textured and untextured moving surfaces. For $Re^* < 0.001$, there is no influence on the results. However, for $Re^* > 0.001$, a low aspect ratio ($C = 80$ [μm], $h_p = 30$ [μm]) and a moving textured surface, the results are affected by $Re^*$ and the

detrimental effect increases. Figure 8b–d present bottom-view pressure distributions for this case at the textured surface for different values of $Re^*$ in one of the dimples. As was observed in [22], the local pressure gradient in the dimple increases as $Re^*$ increases. For $Re^* = 0.01$, the local pressure gradient is significantly bigger and therefore the overall detrimental effect of the texturing is bigger. The significant influence of $Re^*$ indicates that the Reynolds equation may not be valid for modeling surface texturing (which is similar to the conclusions in [15]), even for low values of the Reynolds number. The results in this study are limited to $Re^* < 0.001$ and therefore for lubrication applications with relatively big clearances or velocities, resulting in higher values of $Re^*$ and low aspect ratios for the dimples; the influence of $Re^*$ may affect the results and this should be considered.

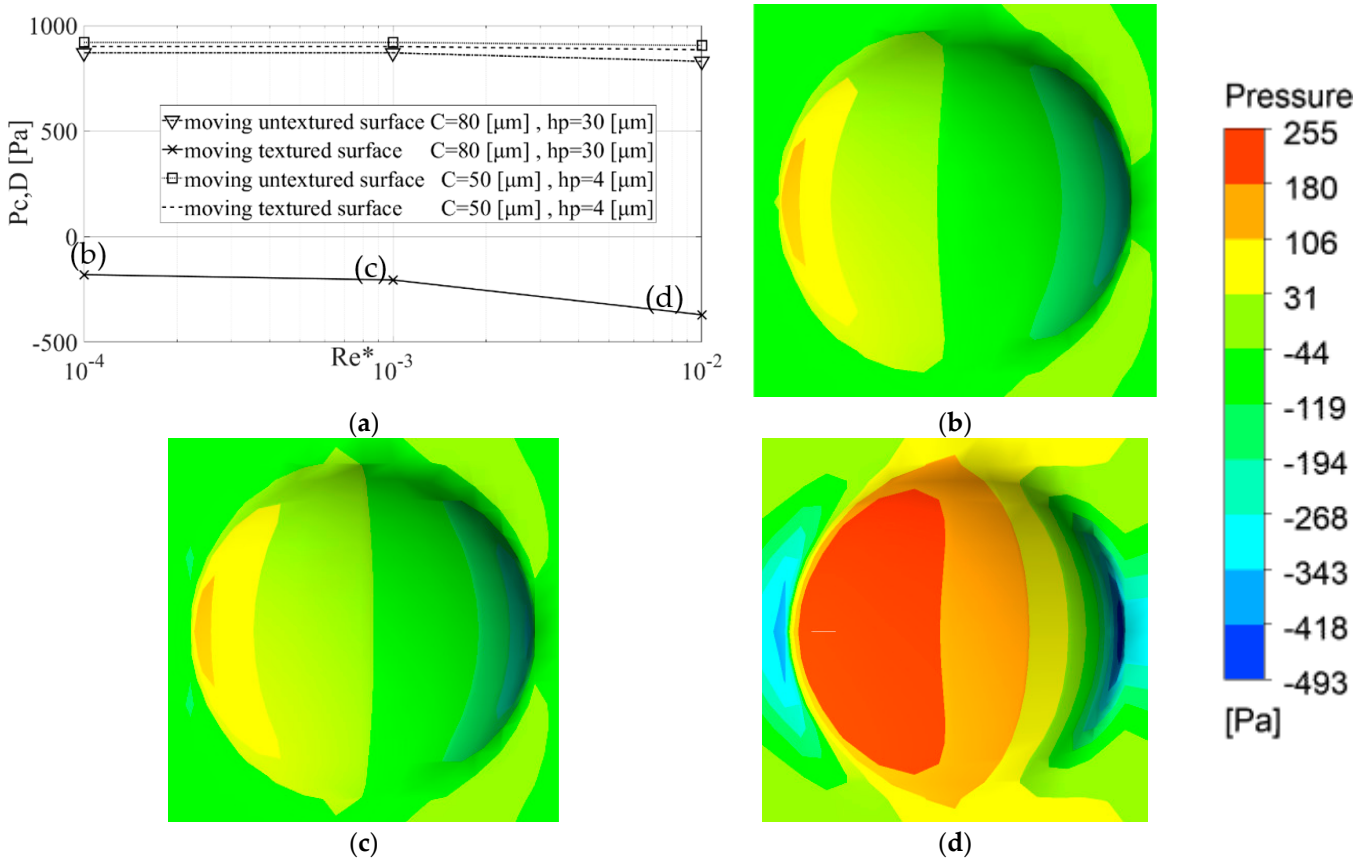


**Figure 8.** Local gage pressure at (**a**) the end of the texturing zone, $P_{c,D}$ versus the reduced Reynolds number, $Re^*$, for various cases and the distribution of the local pressure on the textured surface at one of the dimples for (**b**) $Re^* = 0.0001$, (**c**) $Re^* = 0.001$ and (**d**) $Re^* = 0.01$.

In order to provide general conclusions in dimensionless terms, in the following it is shown that the same dimensionless parameters lead to the same dimensionless results. The dimensionless pressure is presented as the relative difference between the pressure obtained by the dimples and by the equivalent step, $(P_{c,S} - P_{c,D})/P_{c,S}$, and by that it represents the efficiency reduction of the dimples compared with the equivalent step. Figure 9 presents the efficiency reduction for a typical set of dimensionless parameters for moving textured and untextured surfaces as a function of the dimension clearance, $C$. The results show that for a wide range of $C$ ($1\ [\mu m] < C < 100\ [\mu m]$), a universal solution can be obtained; therefore, the conclusions can be discussed in terms of dimensionless parameters.

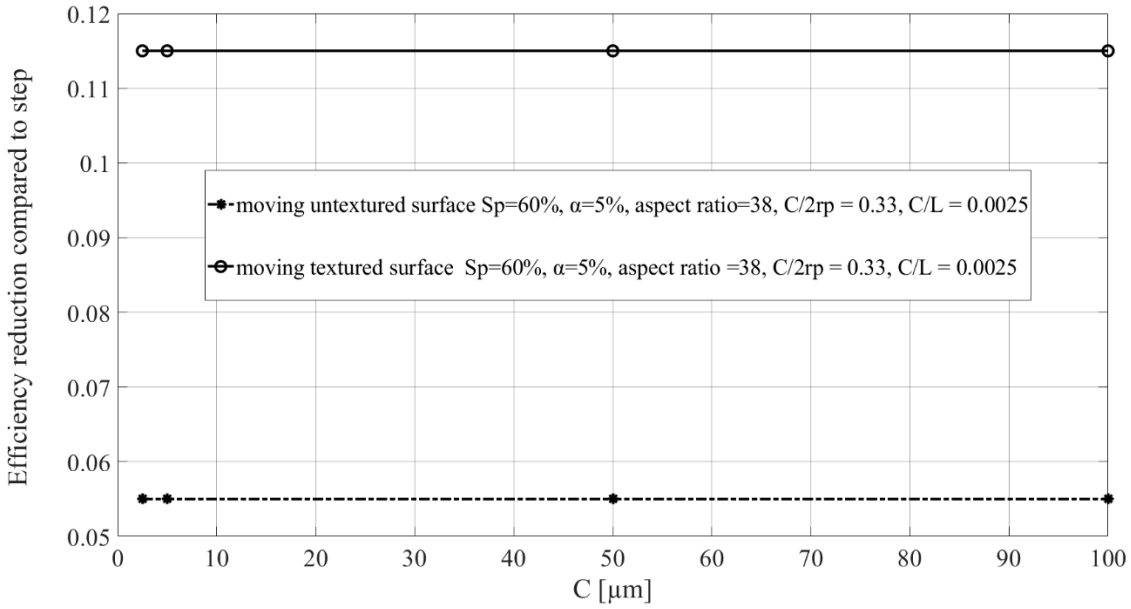


**Figure 9.** Efficiency reduction of the dimples compared with the step for a typical set of dimensionless parameters versus clearance, $C$.

In Figure 10, the pressure distribution in the gap is presented for dimple density, $S_p = 5\%$. Even though $S_p$ is low, the pressure distribution is similar to the Rayleigh step bearing. Figure 11a presents the effect of $S_p$ on the efficiency reduction for $C = 50[\mu m]$, $h_p = 10[\mu m]$ and $C = 20[\mu m]$, $h_p = 4[\mu m]$ for textured and untextured moving surfaces. The other parameters are the same as in Table 2. As was observed in [12], there is no optimum for $S_p$. In other words, an increase in the density reduces the efficiency. However, the effect is small, and even for low densities, the equivalent step (which is shallower for low density) can be used for simulating dimple texturing. Figure 11b presents the effect of the texturing portion, $\alpha$, on the efficiency reduction. It seems that the relative difference does not depend on the texturing portion. Further results show that the ratio between the dimple radius and the length of the model, $r_p/L$, has no effect on the efficiency reduction.

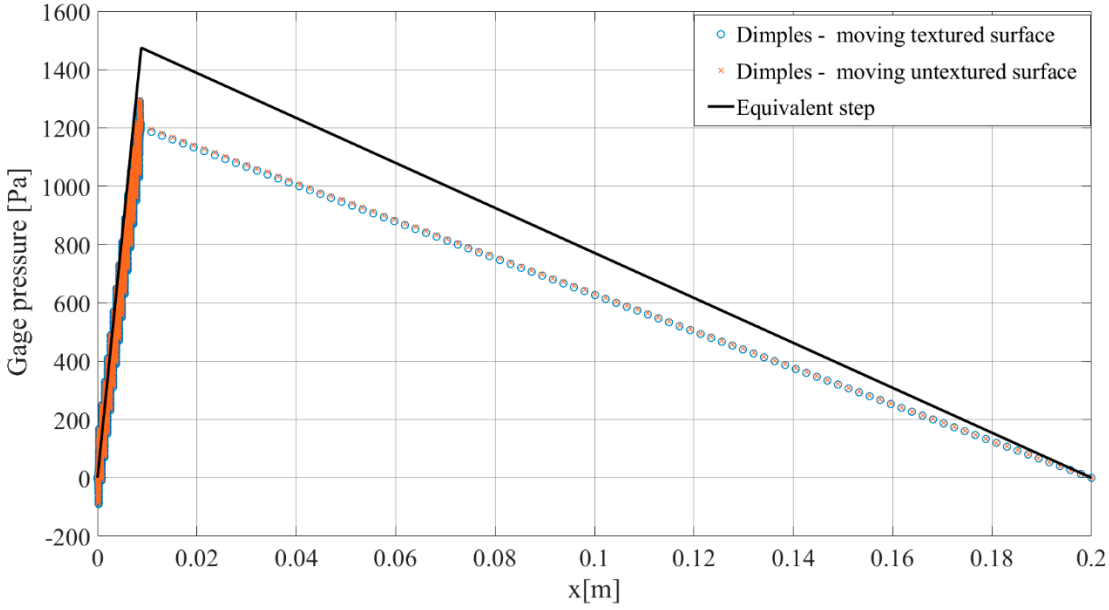


**Figure 10.** Distribution of local pressure for $C = 50[\mu m]$, $h_p = 4[\mu m]$ and $S_p = 5\%$. Dimple texturing and equivalent step.

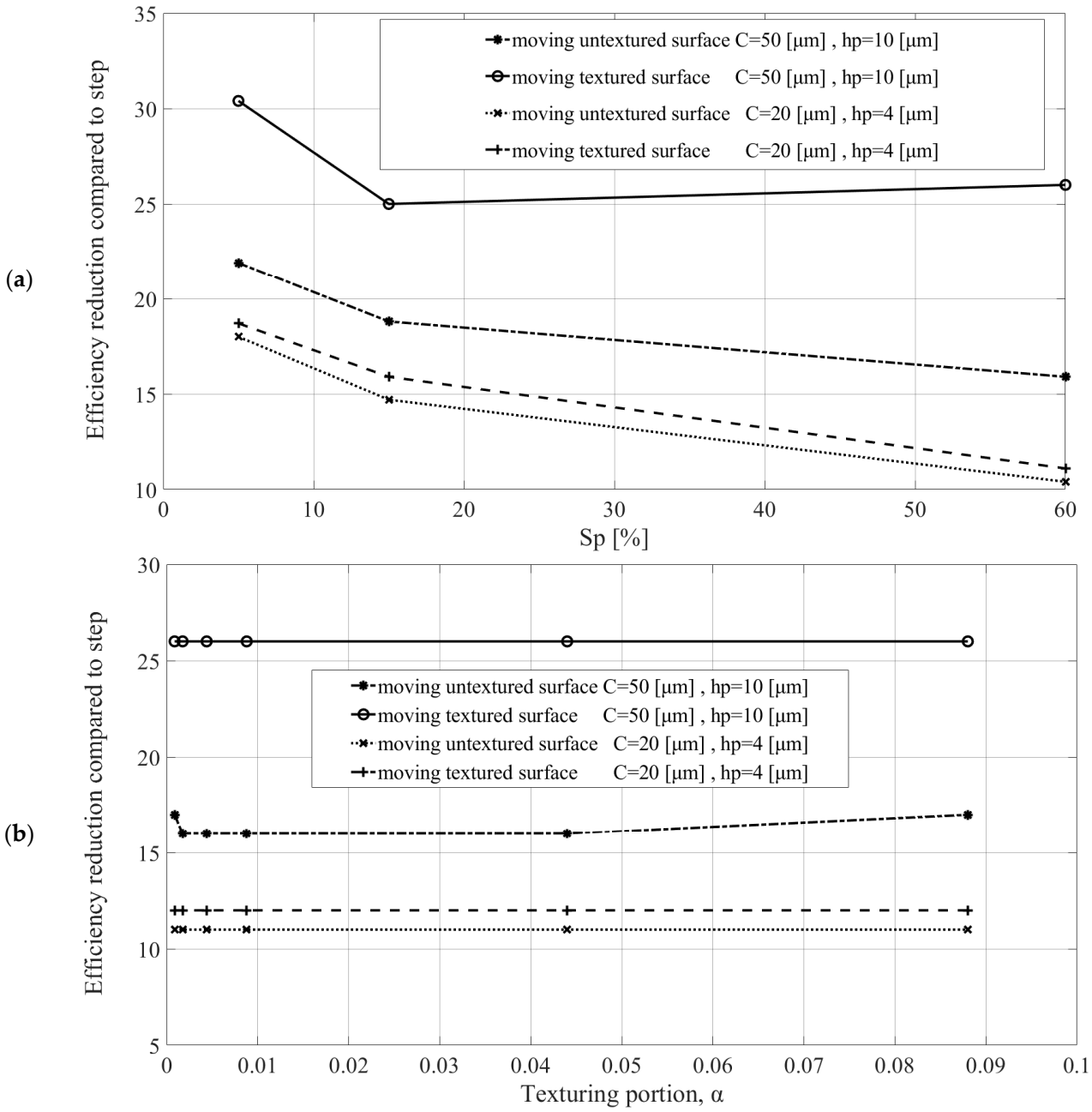


**Figure 11.** Efficiency reduction versus (**a**) dimple area density, $S_p$, (**b**) texturing portion, α, various cases.

Figure 12 presents the effect of the dimensionless clearance, $C/2r_p$, and the aspect ratio, $2r_p/h_p$, on the efficiency reduction for both textured and untextured moving surfaces. The results for both cases show that for relatively low values of $C/2r_p$, the efficiency reduces (derives from the left side of the maps). For higher values, $C/2r_p$ does not affect the efficiency reduction for moving untextured surfaces. However, for moving textured surfaces, the efficiency reduces as $C/2r_p$ increases. The reason for this might be because for this case (unlike the untextured moving surface case), an increase in the clearance leads to increased velocities for the fluid inside the dimple, which has a detrimental effect, as mentioned above (see Figure 7). In addition, for both cases, low values of $2r_p/h_p$ lead to a significant efficiency reduction. In the case of a moving untextured surface, in the range $2r_p/h_p > 15$, $C/2r_p > 0.15$, there is a good match between the dimples and the equivalent step (efficiency reduction of less than 20%). In the case of a moving textured surface,

there is only a small range of parameters with a good match and therefore the equivalent step cannot be used for simulating dimple texturing for the majority of hydrodynamic lubrication applications. However, the efficiency reduction that is presented in the current study can be used to estimate the pressure distribution for a textured surface for a wide range of parameters. For big clearances and small aspect ratios, the differences can be more than 100%. For these cases, the gage pressure is negative and the texturing is detrimental.

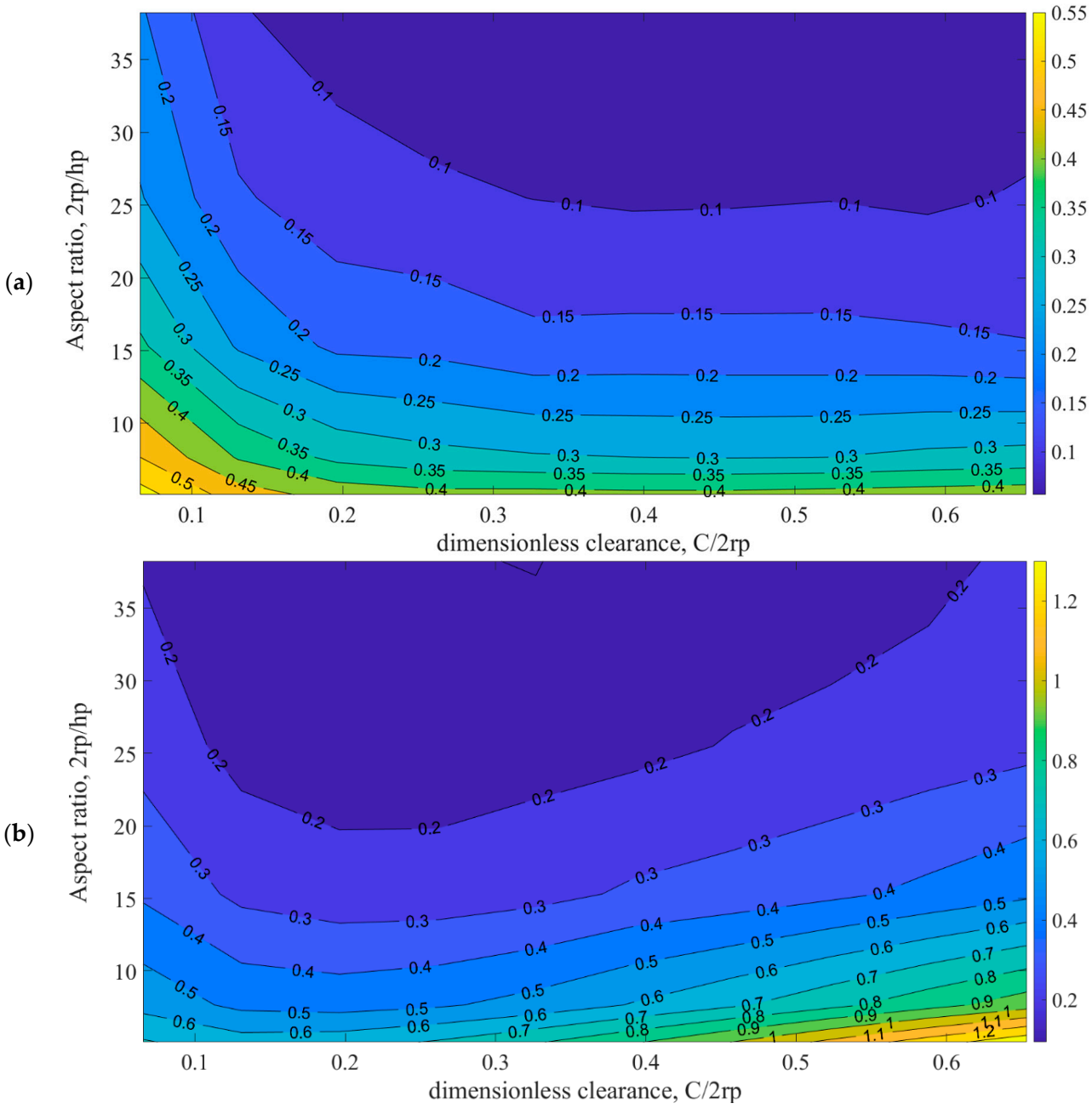


**Figure 12.** Efficiency reduction versus dimensionless clearance, $C/2r_p$, and aspect ratio, $2r_p/h_p$, for (**a**) a moving untextured surface and (**b**) a moving textured surface.

### *4.3. Pressure-Drop-Induced Flow*

In this section $\Delta P = 1$ [Mpa] and $U = 0$. For an untextured surface, the pressure distribution is linear. For a step profiled surface, the pressure distribution is bilinear and the pressure at end of the texturing portion is higher than the for the linear case (for a step located close to the inlet). In Figure 13a, the pressure distribution in the gap for the dimple-textured surface, the equivalent volume step and the untextured surface are presented for

$C = 100$ [μm], $h_p = 20$ [μm] and in Figure 13b for $h_p = 57$ [μm]. The other parameters are the same as in Table 2. The results show that the pressure for the textured surface is higher than the untextured surface but lower than the stepped profiled surface (the dimples are less effective than the equivalent step). However, for $h_p = 20$ [μm], the difference between the textured and the step profiled surfaces is small, and even though the aspect ratio of the dimples is low (less than 8), there is a good match between the results. A variety of dimple parameters were examined, and it was found that for $10[\mu m] < C < 100[\mu m]$ and $2r_p/h_p > 7.5$, there is a good agreement. For lower aspect ratios (deeper dimples), the dimple texturing is significantly less effective than the equivalent step. However, there is some improvement compared with the linear case, as depicted in Figure 13b.

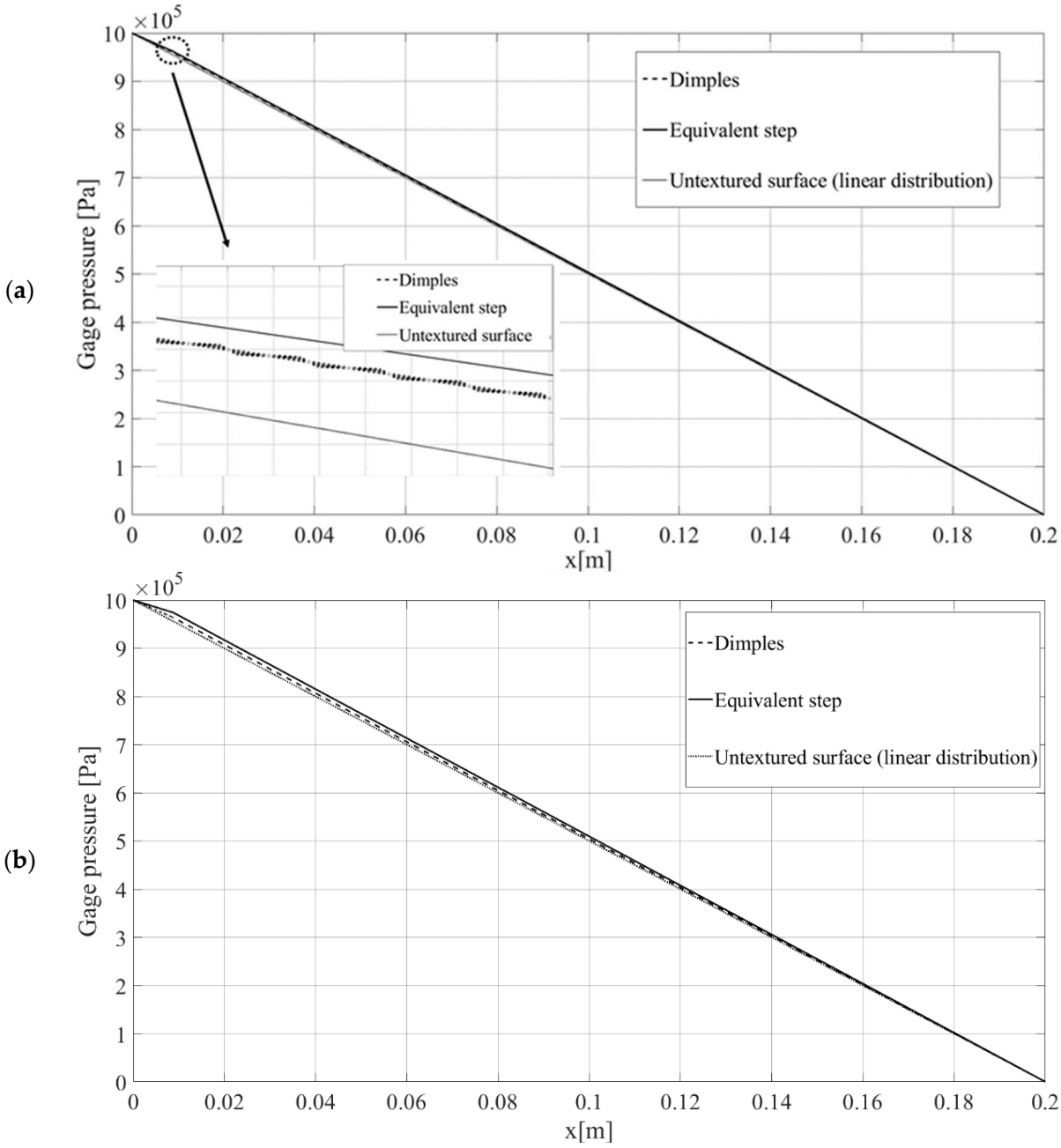


**Figure 13.** Typical distributions of local pressure for (**a**) $C = 100$ [μm], $h_p = 20$ [μm] and (**b**) $C = 100$ [μm], $h_p = 57$ [μm]. Dimple texturing, equivalent step and untextured surfaces.

## 5. Conclusions

The effect of partial surface texturing on mating surfaces was studied. A simplified model using one partially textured row of dimples with symmetry boundary conditions was used. This model can be used to simulate various of hydrodynamic lubrication applications. The model was verified vs. experimental and theoretical studies from the literature for both partial texturing and full texturing. The results indicate that the Reynolds equation that was used in the literature for full texturing is not applicable.

In the current study, the velocity was applied either to the textured surface or to the untextured surface. The pressure distribution in the gap was compared with the pressure distribution of an equivalent volume step. It was found that partial surface texturing was less effective than the equivalent step, especially for moving textured surfaces.

The effect of the reduced Reynolds number, $\mathrm{Re}^*$, was examined, and it seems that the effect of $\mathrm{Re}^*$ for a low aspect ratio and a moving textured surface is significant and cannot be neglected even for low values of $\mathrm{Re}^*$ ($\mathrm{Re}^* < 0.01$).

The efficiency reduction of the dimples in comparison with the equivalent step was examined. It was found that there are three parameters that affect the efficiency reduction. The most important parameter is the aspect ratio, $2r_\mathrm{p}/h_\mathrm{p}$. For both moving textured and untextured surfaces, high values for the aspect ratio lead to a small efficiency reduction, whereas low values for the aspect ratio lead to a large reduction. The second important parameter is the dimensionless clearance, $C/2r_\mathrm{p}$. For both cases, small values of $C/2r_\mathrm{p}$ lead to a large efficiency reduction. For the moving untextured surface, high values of $C/2r_\mathrm{p}$ do not affect the efficiency reduction, whereas for the moving textured surface, increasing $C/2r_\mathrm{p}$ reduces the efficiency. A map is provided for both cases that can be used for estimating the efficiency reduction for different aspect ratios and different dimensionless clearances. The third parameter is the dimple density. A high density for the dimples leads to a smaller efficiency reduction. However, the effect is small and even a low density for the dimples leads to a Rayleigh-step-like pressure distribution. Two additional parameters were examined—the texturing portion, $\alpha$, and the ratio between the dimple radius and the length of the model, $r_\mathrm{p}/L$; it was found that they have no effect on the efficiency reduction.

For a moving textured surface, a small aspect ratio (deep dimples) and relatively big clearances may result in negative gage pressure (detrimental effect). Furthermore, the influence of the dimples on the fluid flow was observed, and it seems that the high velocities in the gap direction caused by the motion of the textured surface affects the flow and hence leads to negative gage pressure. The shape of the dimples may affect the velocities in the gap direction and therefore should be examined.

For pressure-drop-induced flow, it was found that the pressure distribution of the dimple texturing is similar to the pressure distribution of the equivalent step for a wide range of parameters.

The current simulation approach in this study does not consider interactions between the fluid and the material of the surfaces since it focuses on the pressures and velocities of the fluid. These interactions can modify the surface topology and should be considered in future work.

**Author Contributions:** Conceptualization, I.C. and R.G.; methodology, I.C. and R.G.; writing—original draft preparation, I.C.; writing—review and editing, R.G.; supervision, R.G. All authors have read and agreed to the published version of the manuscript.

**Funding:** This research received no external funding.

**Institutional Review Board Statement:** Compliance with ethical standards.

**Data Availability Statement:** Not applicable.

**Acknowledgments:** This paper is part of the IEA AMT IA technical activities.

**Conflicts of Interest:** The authors declare no conflict of interest.

## Nomenclature

| | |
|---|---|
| $C$ | Clearance between the surfaces |
| $L$ | Length of the surface |
| $\alpha$ | Texturing portion |
| $r_p$ | Dimple base radius |
| $h_p$ | Dimple depth |
| $V_p$ | Dimple volume |
| $2r_b$ | Imaginary square cell length |
| $S_p$ | Dimple density |
| $h_S$ | Step depth |
| $P_1$ | Pressure on the inlet |
| $P_2$ | Pressure on the outlet |
| $\Delta P$ | Pressure drop |
| $P_c$ | Pressure at the end of the texturing zone |
| $q$ | Mass flow rate per unit of width |
| x, y | Coordinates |
| $x^*$ | Dimensionless coordinate |
| $U$ | x-Velocity |
| $\rho$ | Density of the fluid |
| $\mu$ | Viscosity of the fluid |
| $Re^*$ | Reduced Reynolds number |
| $h$ | Local clearance between the surfaces |
| $p$ | Local pressure of the fluid |
| $p^*$ | Dimensionless pressure |

## References


1. Vishnoi, M.; Kumar, P.; Murtaza, Q. Surface Texturing Techniques to Enhance Tribological Performance: A Review. *Surf. Interfaces* **2021**, *27*, 101463. [CrossRef]
2. Lu, P.; Wood, R.J.K. Tribological Performance of Surface Texturing in Mechanical Applications—A Review. *Surf. Topogr.* **2020**, *8*, 43001. [CrossRef]
3. Gropper, D.; Wang, L.; Harvey, T.J. Hydrodynamic Lubrication of Textured Surfaces: A Review of Modeling Techniques and Key Findings. *Tribol. Int.* **2016**, *94*, 509–529. [CrossRef]
4. Tønder, K. Hydrodynamic Effects of Tailored Inlet Roughnesses: Extended Theory. *Tribol. Int.* **2004**, *37*, 137–142. [CrossRef]
5. Kumar, V.; Verma, R.; Kango, S.; Sharma, V.S. Recent Progresses and Applications in Laser-Based Surface Texturing Systems. *Mater. Today Commun.* **2021**, *26*, 101736. [CrossRef]
6. Etsion, I. Modeling of Surface Texturing in Hydrodynamic Lubrication. *Friction* **2013**, *1*, 195–209. [CrossRef]
7. Ronen, A.; Etsion, I.; Kligerman, Y. Friction-Reducing Surface-Texturing in Reciprocating Automotive Components. *Tribol. Trans.* **2001**, *44*, 359–366. [CrossRef]
8. Etsion, I. State of the Art in Laser Surface Texturing. *J. Tribol.* **2005**, *127*, 248–253. [CrossRef]
9. Etsion, I.; Kligerman, Y.; Halperin, G. Analytical and Experimental Investigation of Laser-Textured Mechanical Seal Faces. *Tribol. Trans.* **1999**, *42*, 511–516. [CrossRef]
10. Wang, W.; Liu, Z.; Chen, D.; Xie, Z.; Song, J. Influence of Different Surface Texture Parameters on the Contact Performance of Piston Ring-Sleeve Friction Pair of Hydraulic Cylinders. *Adv. Mater. Sci. Eng.* **2021**, *2021*, 5495995. [CrossRef]
11. Etsion, I.; Halperin, G. A Laser Surface Textured Hydrostatic Mechanical Seal. *Tribol. Trans.* **2002**, *45*, 430–434. [CrossRef]
12. Brizmer, V.; Kligerman, Y.; Etsion, I. A Laser Surface Textured Parallel Thrust Bearing. *Tribol. Trans.* **2003**, *46*, 397–403. [CrossRef]
13. Kligerman, Y.; Etsion, I.; Shinkarenko, A. Improving Tribological Performance of Piston Rings by Partial Surface Texturing. *J. Tribol.* **2005**, *127*, 632–638. [CrossRef]
14. Pinkus, O.; Sternlicht, B. *Theory of Hydrodynamic Lubrication*; McGraw-Hill: New York, NY, USA, 1961. [CrossRef]
15. Dobrica, M.B.; Fillon, M. About the Validity of Reynolds Equation and Inertia Effects in Textured Sliders of Infinite Width. *Proc. Inst. Mech. Eng. Part J J. Eng. Tribol.* **2009**, *223*, 69–78. [CrossRef]
16. Li, J.; Chen, H. Evaluation on Applicability of Reynolds Equation for Squared Transverse Roughness Compared to CFD. *J. Tribol.* **2007**, *129*, 963–967. [CrossRef]
17. Feldman, Y.; Kligerman, Y.; Etsion, I.; Haber, S. The Validity of the Reynolds Equation in Modeling Hydrostatic Effects in Gas Lubricated Textured Parallel Surfaces. *J. Tribol.* **2006**, *128*, 345–350. [CrossRef]
18. Wei, S.; Kligerman, Y.; Goltsberg, R. Reverse Flow in Submerged Journal Bearings. *Tribol. Trans.* **2023**, *66*, 162–174. [CrossRef]
19. Wei, S.; Kligerman, Y.; Goltsberg, R.; Etsion, I. Variation of Lubricant Distribution Across the Radial Direction in a Journal Bearing. *J. Tribol.* **2022**, *144*, 061803. [CrossRef]

20. Cohen, I.; Kligerman, Y.; Goltsberg, R. CFD Analysis of a Ringless Piston's Secondary Motion and the Validity of Reynolds Equation. *Meccanica* **2023**, *58*, 1347–1364. [CrossRef]
21. Yong, H.; Balendra, R. CFD Analysis on the Lubrication Behaviours of Journal Bearing with Dimples. In Proceedings of the 2009 IEEE International Conference on Mechatronics and Automation, Changchun, China, 9–12 August 2009; ISBN 9781424426935.
22. Li, K.; Jing, D.; Hu, J.; Ding, X.; Yao, Z. Numerical Investigation of the Tribological Performance of Micro-Dimple Textured Surfaces under Hydrodynamic Lubrication. *Beilstein J. Nanotechnol.* **2017**, *8*, 2324–2338. [CrossRef]
23. Abdul Rahman, H.; Ghani, J.A.; Wan Mahmood, W.M.F.; Mohammad Rasani, M.R. Computational Fluid Dynamic Study on the Tribological Performance of Dimple-Textured Surface Fabricated Using the Turning Process. *Ind. Lubr. Tribol.* **2019**, *71*, 594–602. [CrossRef]
24. Liu, W.; Ni, H.; Chen, H.; Wang, P. Numerical Simulation and Experimental Investigation on Tribological Performance of Micro-Dimples Textured Surface under Hydrodynamic Lubrication. *Int. J. Mech. Sci.* **2019**, *163*, 105095. [CrossRef]
25. Kligerman, Y.; Etsion, I. Analysis of the Hydrodynamic Effects in a Surface Textured Circumferential Gas Seal. *Tribol. Trans.* **2001**, *44*, 472–478. [CrossRef]
26. Hamrock, B.J.; Schmid, S.R.; Jacobson, B.O. *Fundamentals of Fluid Film Lubrication*; CRC Press: New York, NY, USA, 2004.
27. Kligerman, Y.; Cohen, I.; Shinkarenko, A. Centering and Friction Reduction between Parts of the Cylinder-Piston Group. In Proceedings of the 10th International Scientific Conference BALTTRIB 2019, Kaunas, Lithuania, 14–16 November 2019; pp. 94–101. [CrossRef]
28. Fluent, A. *Ansys Fluent Theory Guide*, 15th ed.; ANSYS Inc.: Canonsburg, PN, USA, 2013.